metals

MDPI

Article

Boosting Electrocatalytic Reduction of Nitrate to Ammonia over Co_3O_4 Nanosheets with Oxygen Vacancies

Xing Wu [1], Zhigong Liu [1], Tianyu Gao [1], Zhizhuo Li [1], Zhenhui Song [1], Jia Tang [1], Fan Feng [1], Caiyan Qu [1], Fubing Yao [1,2,3,*] and Chongjian Tang [1,2,3,*]

1 School of Metallurgy and Environment, Central South University, Changsha 410083, China
2 Chinese National Engineering Research Center for Control & Treatment of Heavy Metal Pollution, Changsha 410083, China
3 State Key Laboratory of Advanced Metallurgy for Non-Ferrous Metals, Changsha 410083, China
* Correspondence: yaofubing@csu.edu.cn (F.Y.); chjtang@csu.edu.cn (C.T.)

Abstract: Electrocatalytic nitrate reduction into ammonia is promising for its restricted activity and selectivity in wastewater treatment, however, it remains challenging. In this work, Co_3O_4 nanosheet electrodes with rich oxygen vacancies (OVs) (Co_3O_{4-x}/NF) are prepared and then applied as efficient catalysts for selective electrocatalytic reduction of nitrate to ammonia. The resulting Co_3O_{4-x}/NF electrodes exhibit high NO_3^--N removal efficiency and NH_4^+-N selectivity, at 93.7% and 85.4%, respectively. X-Ray photoelectron spectroscopy (XPS) and electron paramagnetic resonance spectra (EPR) results clearly reveal the formation of OVs in Co_3O_{4-x}/NF. The electrochemical characterization results confirm that OVs can effectively improve electron transfer as well as the electrochemically active area. The Co^{2+}/Co^{3+} ratio of Co_3O_{4-x}/NF increases after the electrocatalytic reduction of nitrate, highlighting the crucial role played by Co^{2+} in mediating ammonia production via the Co^{2+}/Co^{3+} cycle. These findings offer valuable guidelines for the development of more efficient and sustainable approaches for nitrate-contaminated wastewater treatment and ammonia synthesis.

Keywords: electrocatalysis; nitrate; ammonium; Co_3O_4; oxygen vacancies

check for updates

Citation: Wu, X.; Liu, Z.; Gao, T.; Li, Z.; Song, Z.; Tang, J.; Feng, F.; Qu, C.; Yao, F.; Tang, C. Boosting Electrocatalytic Reduction of Nitrate to Ammonia over Co_3O_4 Nanosheets with Oxygen Vacancies. *Metals* **2023**, *13*, 799. https://doi.org/10.3390/met13040799

Academic Editor: Leonid M. Kustov

Received: 16 March 2023
Revised: 8 April 2023
Accepted: 17 April 2023
Published: 18 April 2023

1. Introduction

Acid rain deposition of nitrogen oxides from the combustion of nitrogen-containing fuels, bacterial decomposition of nitrogen-containing fertilizers, and discharge of nitrate-containing domestic and industrial wastewater are all highly likely to lead to elevated nitrate concentrations in groundwater [1–3]. Nitrate (NO_3^-) levels must be restricted to ensure a balanced ecosystem, otherwise, they can lead to environment pollution (e.g., eutrophication) and threaten the health of human beings (e.g., blue baby syndrome) [4–6]. Thus, significant efforts to remove NO_3^- have led to the development of a number of concepts and techniques, such as ion exchange, reverse osmosis, biological denitrification, electrodialysis, etc. [7–14]. Although these methods have proven to be efficient technologies for treating certain conditions, they may require significant capital investment. For instance, chemical or biological treatment processes may necessitate the use of reducing agents such as H_2 or acetic acid that serve as electron donors [15,16]. Recognizing the significance of nitrogen (N) is crucial, as it serves as an essential nutrient for plant growth and plays a key role in the production of industrial products [17–19]. As such, recovery or extraction of N from NO_3^- is greatly beneficial for both sustainable agriculture and industrial production. Unfortunately, current methods for treating waste water result in the conversion of NO_3^- to nitrogen gas, resulting in the loss of valuable nitrogen resources. Therefore, developing methods for recovery of N resources from NO_3^--contaminated water is critical for both sustainable development and environmental protection.

Currently, the electrocatalytic nitrate reduction reaction (NO_3RR) is generally considered an efficient method for remediating wastewater, with benefits including absence of

chemical waste byproduct streams and lower capital costs; thus, it has attracted increasing attention. Importantly, high-value-added products such as ammonia (NH_3) can be the harvesting indication for NO_3^-RR process [11,20,21]. It is well known that the Haber–Bosch process is the primary method of NH_3 production; this process, however, requires significant energy (~2% of the world's energy) and emits a substantial amount of greenhouse gases (~1.5% of global carbon dioxide emissions) [22,23]. As a result, NO_3RR may be an alternative approach for producing NH_3 through a more sustainable and environmentally friendly manner while helping to solve water pollution challenges.

The electrocatalyst, an essential component of NO_3RR, directly impacts the rate of NO_3^- removal and selectivity of the NH_3 yield. Therefore, the rational design and development of high-performance electrocatalysts is crucial for achieving efficient and selective NO_3RR. Recently, electrocatalysts made of noble metals (e.g., Ru, Pd, and Pt) have been explored and found to exhibit high performance for NH_3 production by NO_3RR; however, undesirable capital output hinders their application [24–26]. Transition metal-based nanocatalysts represent an effective alternative to noble metal catalysts, and have gained significant attention for NH_3 production via NO_3RR owing to their low cost and abundance [27,28]. Among them, Co_3O_4 nanocomposite is considered a promising electrocatalyst due to its impressive catalytic properties [29]. Unfortunately, the widespread use of Co_3O_4 is limited by its poor electrical conductivity [30]. Recently, oxygen vacancies (OVs) have been demonstrated to modulate its electronic states, significantly altering catalytic activity [31]. For instance, Jia and co-workers found that the introduction of O-vacancies into TiO_2 nanotubes could significantly enhance the performance of electrodes used for synthesis of NH_3 from NO_3^- through electrochemical reduction [3]. Meanwhile, previous studies have demonstrated that the embedding of OVs affects the proportion of Co^{2+} and Co^{3+} in Co_3O_4 [32]. Notably, it has been reported that Co^{2+} can serve as an electron donor for NO_3^- reduction during the electrochemical reaction process. Therefore, it is reasonable to expect introduction of OVs into Co_3O_4 nanostructures with given facets to be a promising electrocatalyst for NH_3 production via NO_3RR.

In this work, OV-rich Co_3O_4 nanosheets grown on the surface of nickel foam (Co_3O_{4-x}/NF) were synthesized via NO_3^- electroreduction for use in NH_3 production. X-Ray photoelectron spectroscopy (XPS) and electron paramagnetic resonance spectra (EPR) confirmed that abundant OVs were present in the Co_3O_{4-x}/NF. Benefiting from the improved electronic structure and Co^{2+}/Co^{3+} ratio of Co_3O_4 after the introduction of OVs, the electrocatalyst exhibited high activity vs. Ag/AgCl at −1.2 V, with 93.7% NO_3^--N removal efficiency and 85.4% NH_4^+-N selectivity. When comparing the states before and after the reaction, a significant change in the Co^{2+}/Co^{3+} ratio was found, indicating that NH_3 production from NO_3RR was mediated by the Co^{2+}/Co^{3+} cycle. This study is believed to be a feasible reference that can help to realize utilization of NO_3^- wastewater resources.

2. Materials and Methods

2.1. Chemicals and Reagents

Analytical-grade $NaNO_3$, $NaNO_2$, $(NH_4)_2SO_4$, and Na_2SO_4 were purchased from Kermel Chemical Reagent Co. Ltd. (Tianjin, China) and used to prepare the stock solution. All solutions were prepared using ultrapure water. Nickel foam (NF) purchased from Beijing Pengda Hengtai Technology Co., Ltd. (Beijing, China) was employed as the supporter for growing Co_3O_4 and Co_3O_{4-x}. In order to remove the impurities on the surface of the NF, it was rinsed several times with acetone and 1 M HCl, then again with ultrapure water.

2.2. Preparation of Electrodes

A piece of NF (3 cm × 2 cm × 0.1 cm) was first cleaned several times with 1 M HCl, acetone, ethanol, and H_2O to remove impurities. Next, Co_3O_4/NF was synthesized through a hydrothermal and annealing method. In the typical processes, 0.4202 g of $CoSO_4{\cdot}7H_2O$ and 0.36 g of urea were dissolved in 20 mL of H_2O and 20 mL of ethanol, forming a wine-red solution. Afterwards, this solution was transferred to a 100 mL Teflon-lined autoclave

and the cleaned NF was simultaneously soaked in the mixture. After standing for 12 h without stirring, the Teflon-lined autoclave was heated at 90 °C for 8 h. A pink lump ($2CoCO_3 \cdot 3Co(OH)_2 \cdot H_2O$/NF) was obtained and then calcined at 250 °C for 2 h under N_2 atmosphere to generate Co_3O_4 nanosheet arrays on the NF surface (Co_3O_4/NF). Finally, defect-engineered Co_3O_{4-x}/NF was prepared via immersing the Co_3O_4/NF in 1 M $NaBH_4$ solution for 1 h, then rinsed with deionized water and dried under vacuum at 60 °C for 8 h.

2.3. Electrocatalytic NO_3^- Reduction

Electrocatalytic NO_3^- reduction tests were performed in a three-electrode electrochemical cell with an effective volume of 100 mL controlled by an electrochemical workstation (CHI760E, Shanghai Chenhua, Shanghai, China). The resulting Co_3O_{4-x}/NF material, Ir-Ru/Ti, and saturated Ag/AgCl were used as the working electrode, counter-electrode, and reference electrode, respectively. The gap between each electrode was set to ~1.5 cm. Next, 80 mL of 50 mM Na_2SO_4 solution containing NO_3^- was electrolyzed and stirred at 600 rpm. The cathodic potential was controlled in the range of −0.8~−1.4 V (vs. Ag/AgCl). About 2 mL of reaction solution was taken regularly from the reactor (40 min) to detect the variations in NO_3^-, NO_2^-, and NH_4^+.

2.4. Analytical Methods

An X-Ray photoelectron spectroscopy (XPS) survey of the spectra of Co 2p was carried out using an Escalab 250Xi (Thermol Scientific, Waltham, MA, USA) with an Al/Mg Kα line as the dual X-Ray source. The surface morphology was detected by Scanning Electron Microscopy (SEM, FEI Quanta 200 CZ, FEI, Eindhoven, The Netherlands). X-Ray diffraction (XRD, Ultima IV, Rigaku, Tokyo, Japan) was used to analyze the crystallinity of NF, Co_3O_4/NF, and Co_3O_{4-x}/NF. Materials Data, Inc. (MDI) Jade 5.0 software was used to analyze the diffraction peaks and crystalline phases using the Joint Committee on Powder Diffraction Standards (JCPDS) database as a reference. The electron paramagnetic resonance (EPR) was investigated on a Bruker A300 (Bruker Corporation, Karlsruhe, Germany). Electrochemical testing of the electrochemical impedance spectrum (EIS), linear sweep voltammetry (LSV), and cyclic voltammetry (CV) were carried out using an electrochemical workstation (CHI760E, Shanghai Chenhua, China) in a three-electrode system.

The concentrations of NO_3^- and nitrite (NO_2^-) were measured by Dionex ion-exchange chromatography (ICS-900) with a 0.5 mL sample loop, conductivity suppressor (ASRS 300 × 4 mm), analytical column (AS23 4 × 250 mm), and precolumn (AG23 4 × 50 mm). The eluent (1.0 mL min^{-1}) was set to 9.4 mM sodium carbonate (Na_2CO_3) and1.8 mM sodium bicarbonate ($NaHCO_3$). The ammonia was analyzed by ion chromatography (Dionex ICS-900, Massachusetts, USA) with a 20 μL sample loop, cation self-regenerating suppressor (CSRS ULTRA II, 4 mm), guard column (CS 12A 4 × 250 mm), and analytical column (CG12A 4 × 50 mm); 20 mM methanesulfonic acid was adopted as the eluent at the rate of 1.0 mL min^{-1}. The production of NO and N_2O from the electrocatalytic NO_3^- reduction for the Co_3O_4 electrode was negligible [4]. Herein, NO_3^- reduction ($R_{NO_3^-}(\%)$) and total nitrogen (in this study, the sum of NO_3^-, NO_2^-, and NH_4^+) were respectively calculated according to the following equations:

$$R_{NO_3^-}(\%) = \frac{(NO_3^-)_0 - (NO_3^-)_t}{(NO_3^-)_0} \quad (1)$$

$$S_{NH_4^+}(\%) = \frac{(NH_4^+)_t}{(NO_3^-)_0 - (NO_3^-)_t} \quad (2)$$

where 0 and *t* stand for the initial and final states, respectively.

2.5. Calculation of Average Current Efficiency

Based on the amount of NO_3^- removed and the amount of nitrite (NO_2^-), ammonia, and N_2 generated, the average current efficiency was calculated using the following equations:

$$Q(NO_2^- - N)_t = 2F\left(\frac{C(NO_2^-)_t V}{M}\right) \quad (3)$$

$$Q(NH_4^+ - N)_t = 8F\left(\frac{C(NH_4^+)_t V}{M}\right) \quad (4)$$

$$Q(N_2 - N)_t = 5F\left(\frac{(C(NO_3^-)_0 - (NO_3^-)_t - C(NO_2^-)_t - C(NH_4^+)_t)V}{M}\right) \quad (5)$$

$$Q_t = \int_0^t I\,dt \quad (6)$$

$$\eta = [(Q(NO_2^-)_t + Q(N_2)_t + Q(NH_4^+)_t]/Q_t \times 100\% \quad (7)$$

where η (%) stands for the average current efficiency, Q_t is the total number of electrons at reaction time t (min), $Q(NO_2^-)_t$, $Q(N_2)_t$, and $Q(NH_4^+)_t$ (C) are the electrons consumed during nitrate reduction to nitrite, N_2, and ammonia at time t, respectively, $C(NO_3^-)_0$ (mg N L^{-1}) is the initial concentration of nitrate, $(NO_3^-)_t$, $C(NO_2^-)_t$, and $(NH_4^+)_t$ (mg N L^{-1}) are the concentrations of nitrate, nitrite, and ammonia at time t, respectively, V is the volume of the solution (0.08 L), M is the molar mass of N (14,000 mg mol^{-1}), and F is the Faraday's constant (96,500 C mol^{-1}).

2.6. Electrochemical Active Surface Area Measurement

The electrochemical active surface area (ECSA) was implemented in a three-electrode system at an electrochemical station (CHI760E, Shanghai, China). The working electrode was NF, Co_3O_4/NF, or Co_3O_{4-x}/NF, with an effective geometric surface area of 1 cm^{-2}. Platinum and Ag/AgCl served as the counter and reference electrodes, respectively. The ECSA was obtained according to Equations (8) and (9) [33]:

$$ECSA = R_f S \quad (8)$$

$$R_f = \frac{C_{dl}}{60\ \mu F\ cm^{-2}} \quad (9)$$

where R_f is the roughness factor, S was generally equal to the geometric area of the working electrode (1 cm^{-2}), C_{dl} is the double-layer capacitance, and C_{dl} was estimated by plotting j (mA cm^{-2}) at −0.02 V vs. Ag/AgCl against the scan rate, where j was acquired by Cyclic Voltammetry (CV) measurement under potential windows of −0.08~0 V vs. Ag/AgCl at a given scan rate (5, 10, 15, 20, 25, and 30 mV s^{-1}) (50 mM Na_2SO_4).

3. Results and Discussion

3.1. Characterization

In this work, pristine Co_3O_4 nanosheets supported on nickel foam (Co_3O_4/NF) were synthesized by hydrothermal and annealing methods. To introduce oxygen vacancies into Co_3O_4 NWs, the obtained Co_3O_4/NF was further treated by $NaBH_4$ at room temperature [32]. As shown in Figure 1a–c, as compared to pristine NF, the surface of Co_3O_4/NF was covered with dense nanosheets. It was worth noting that the nanosheet morphology of the as-prepared Co_3O_{4-x}/NF electrode exhibited a hexagonal shape. Meanwhile, Figure 1d shows that the thickness of the Co_3O_4 and Co_3O_{4-x} nanosheets was ~110 nm, indicating that the post-treatment process of $NaBH_4$ did not affect the morphology of Co_3O_4. The crystal structure of the as-prepared samples was analyzed by X-Ray diffraction (XRD).

As shown in Figure 2a, the diffraction peaks of Co_3O_4/NF fully matched the hexagonal Co_3O_4 (PDF#43-1003). Meanwhile, the Co_3O_{4-x}/NF exhibited the same diffraction patterns, showing that our post-treatment process did not damage the phase structure. These results clearly reveal that Co_3O_4 and Co_3O_{4-x} nanosheets with hexagonal morphology were able to be densely grown on the surface of nickel foam. Usually, Co_3O_4 is partially reduced to CoO in the strongly reducing environment formed by $NaBH_4$ [32], which in turn confirms the advantage of our method of introducing defects. As shown in Figure 2b, the XPS spectra of the wide scan clearly show the constituent elements of Co_3O_4/NF and Co_3O_{4-x}/NF, namely, Ni 2p, Co 2p, and O 1s, which is in accordance with the above XRD results. In the XPS spectra of Co 2p (Figure 2c), the two fitting peaks at 780.5 and 782.1 eV are attributed to Co^{3+} and Co^{2+}, respectively [4,34]. Noticeably, the Co^{2+}/Co^{3+} surface ratio of Co_3O_{4-x}/NF was determined to be 1.04, which was higher than that of Co_3O_4/NF (0.78). The electron paramagnetic resonance (EPR) spectra result shows that the value of Co_3O_{4-x}/NF (in g) is 2.0038 (Figure 2d), which was due to the OVs in Co_3O_4 [35]. Therefore, nickel foam electrodes with surfaces covered by Co_3O_4 nanosheets with OVs were successfully prepared.

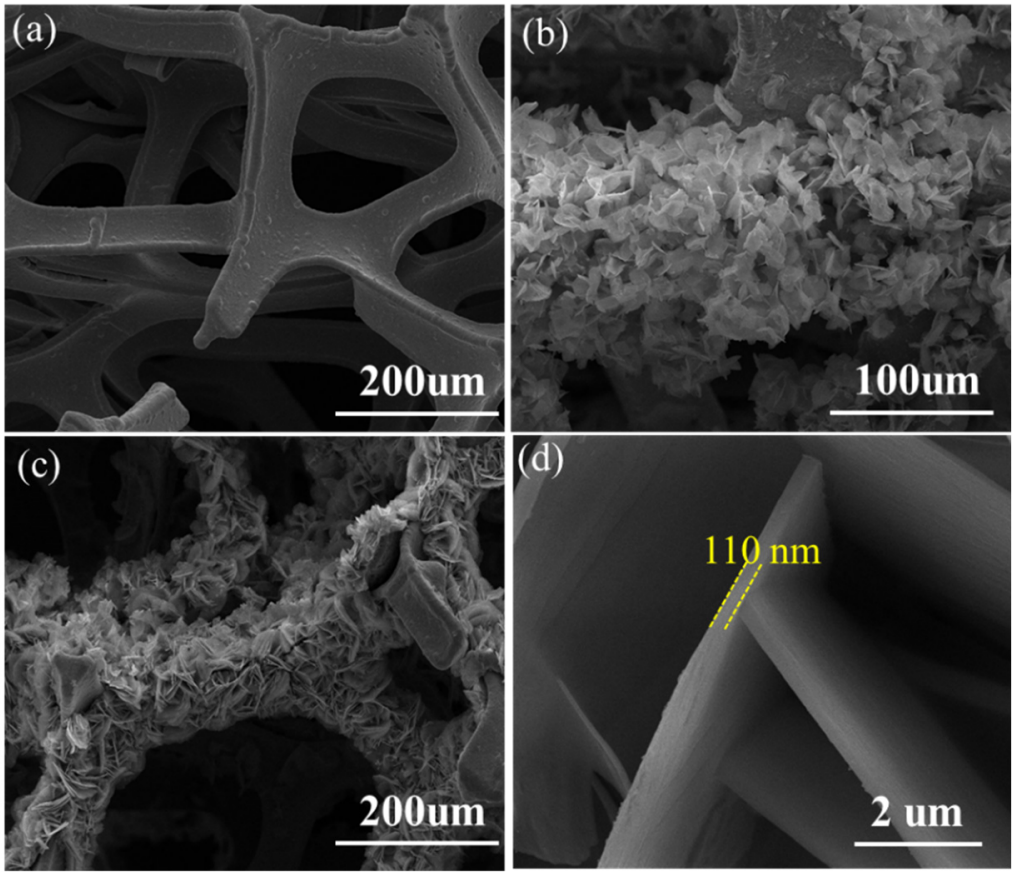

Figure 1. Characterization of as-prepared material: SEM images of NF (**a**), Co_3O_4/NF (**b**), and Co_3O_{4-x}/NF (**c**,**d**).

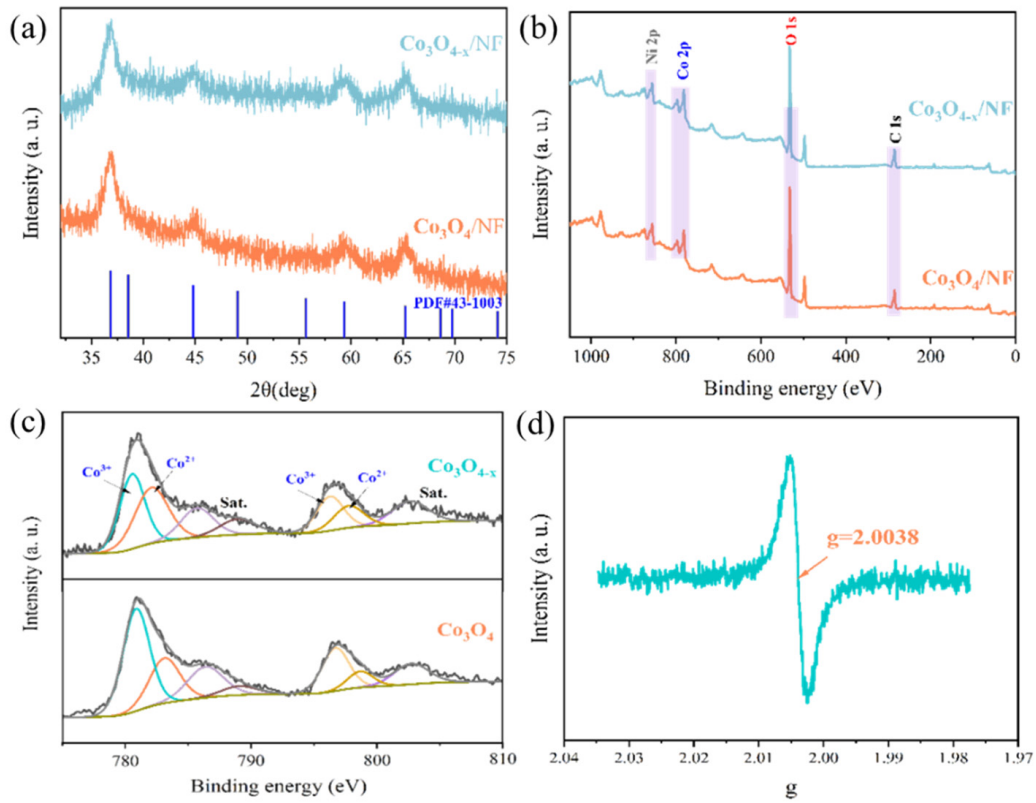

Figure 2. XRD patterns of Co_3O_4/NF and Co_3O_{4-x}/NF (**a**); XPS spectra of wide scan (**b**) and Co 2p (**c**); value of Co_3O_{4-x}/NF (in g) (**d**).

3.2. Electrocatalytic NO_3^- Reduction

The electrocatalytic activities of the electrodes towards NO_3^- reduction were analyzed by LSV, EIS, and C_{dl}. As shown in Figure 3a, the current density observed from −1.0 to −1.2 V vs. Ag/AgCl for Co_3O_{4-x}/NF was lower than that for Co_3O_4/NF, indicating that NO_3^- reduction was more kinetically favorable at the former electrode. EIS can reveal the electron transfer rate in electrochemical reactions based on the arc radius of the Nyquist plot [36]. After reduction by $NaBH_4$, the size of the arc radius decreased (Figure 3b), confirming that the introduction of OVs can reduce the interface impedance and facilitate electron transfer. Accordingly, Co_3O_{4-x}/NF showed higher conductivity and electron transfer properties, which are beneficial to electrochemical NO_3^- reduction through the charge-transfer and mass-transfer processes [37]. It is well known that a larger C_{dl} reflects a higher electrochemical active surface area (ECSA). Figures 3c and S1 show that Co_3O_{4-x}/NF had a C_{dl} value of 6.20 mF cm^{-2}, which was 1.4 and 2.1 times higher than that of NF (4.37 mF cm^{-2}) and Co_3O_4/NF (2.99 mF cm^{-2}), respectively. This increased ECSA can result in enhancement of electrocatalytic active sites, thereby improving electrocatalytic activity for NO_3^- reduction.

The electrocatalytic reduction of NO_3^- was carried out with NF, Co_3O_4/NF, and Co_3O_{4-x}/NF electrodes. Figure 4a shows that 72.7% of NO_3^--N was reduced for Co_3O_4/NF after 280 min of electrolysis. Moreover, NO_3^--N removal efficiency reached up to 93.7% with the Co_3O_{4-x}/NF cathode. On the other hand, only 37.9% of NO_3^- was removed by bare NF, illustrating that the catalytic active sites for NO_3^- reduction were Co_3O_4 and Co_3O_{4-x} rather than NF. Noticeably, the electrocatalytic reduction of NO_3^- with different materials obeyed the pseudo-first-order kinetic model (Figure S2). The corresponding reaction rate constant of NO_3^- reduction with NF, Co_3O_4/NF, and Co_3O_{4-x}/NF was 0.0017, 0.004, and 0.01 min^{-1}, respectively. These results indicate that the Co_3O_{4-x}/NF cathode exhibited the highest electrocatalytic activity for NO_3^- reduction.

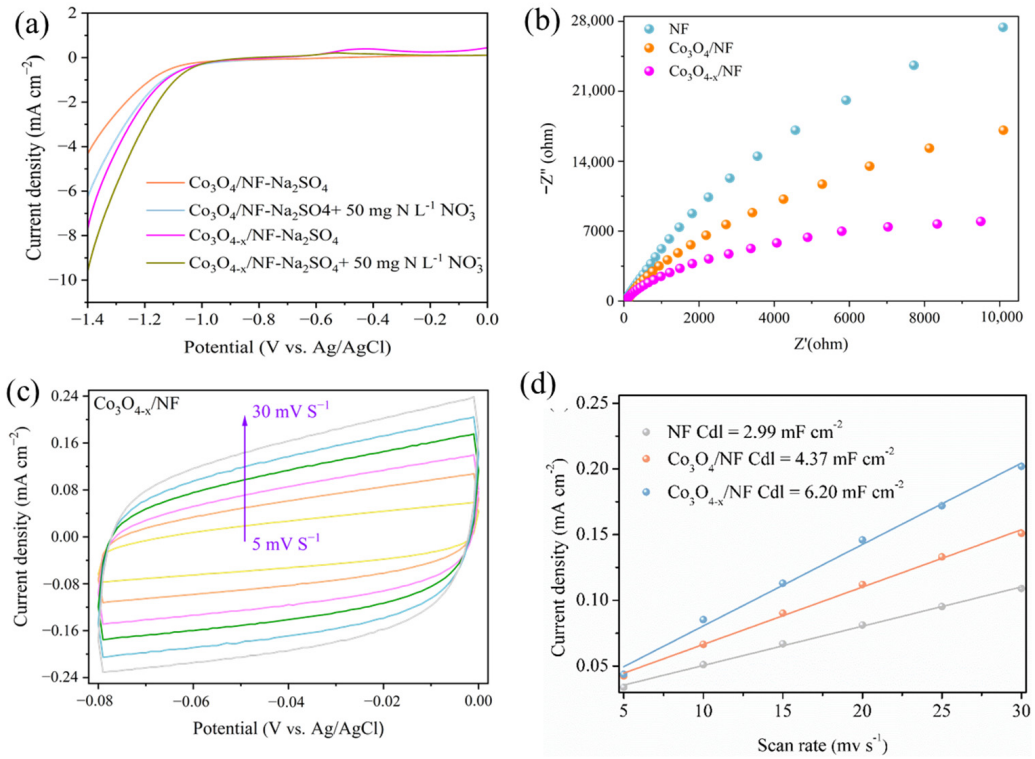

Figure 3. LSV curves of Co_3O_4/NF and Co_3O_{4-x}/NF tested with and without NO_3^--N (**a**); EIS spectra of different electrodes (**b**); CV curves of Co_3O_{4-x}/NF (**c**) in the range of −0.06~0.06 V vs. Ag/AgCl; and linear fitting of the capacitive properties of current density vs. scan rate (**d**).

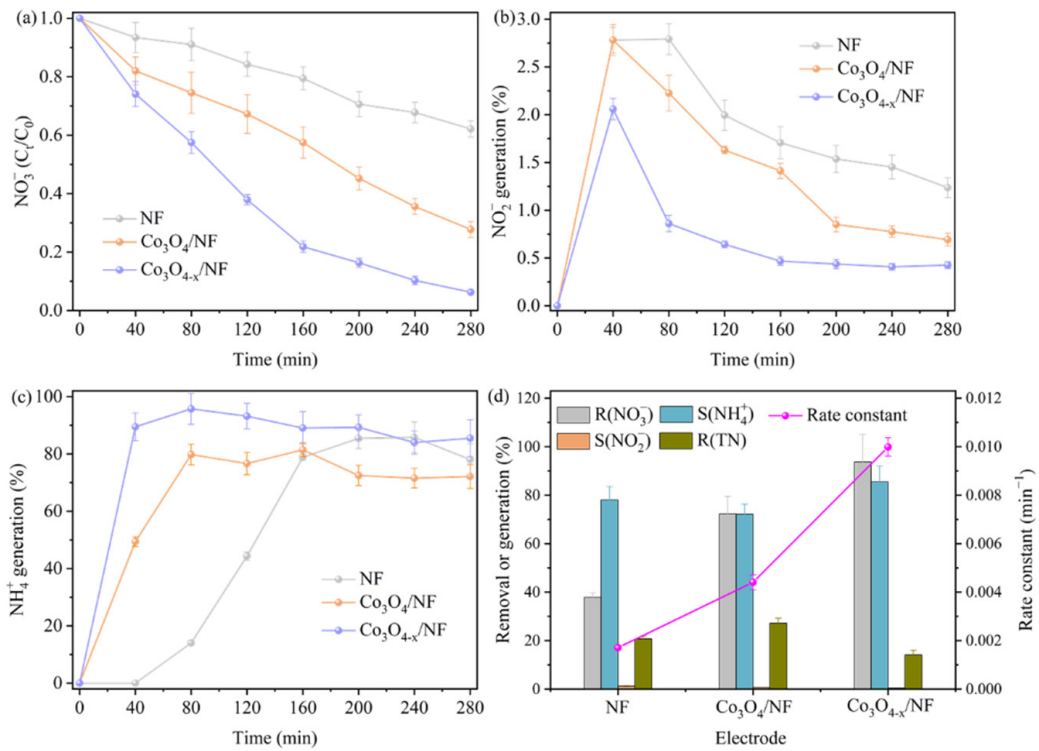

Figure 4. Reduction of NO_3^- (**a**), generation of NO_2^- (**b**) and NH_4^+ (**c**), and TN removal and rate constant (**d**) for different cathodes. Electrolysis conditions: Cathodic potential = −1.2 V (vs. Ag/AgCl), Initial NO_3^- concentration = 50 mg N L^{-1}, Solution volume = 80 mL, pH = 7.0, Stirring rate = 600 rpm, Electrolysis time = 280 min.

The products transformed via NO_3^- reduction on different electrodes were determined comparatively (Figure 4b–d). As shown in Figure 4b, generation of NO_2^- increased first and then decreased, suggesting that NO_2^- was an intermediate product. However, NH_4^+ increased steadily with the reaction time, indicating that it was a final product (Figure 4c). Owing to the faster electron transfer rate and higher ECSA induced by OVs, Co_3O_{4-x}/NF achieved a remarkable 90% NH_4^+-N selectivity in less than 40 min, compared to 0% and 50% for NF and Co_3O_4/NF, respectively. These results fully confirm that Co_3O_{4-x}/NF has outstanding electrocatalytic performance for NO_3RR into NH_3, making it highly suitable for practical applications.

3.3. Effect of Reaction Parameters on Electrocatalytic NO_3^- Reduction

Electrochemical redox reactions are heavily dependent on the electrode potential-. Several potentials (−1.0, −1.1, −1.2, −1.3, and −1.4 V vs. Ag/AgCl) were applied to disclose the effect mechanism of cathodic potential on NO_3RR. As shown in Figure 5a, NO_3^- removal efficiency was 35.8%, 80.7%, 93.7%, 99.6%, and 98.9% at −1.0, −1.1, −1.2, −1.3, and −1.4 V, respectively, indicating that reducing the potential was beneficial for NO_3^- removal, though the effect is not significant below −1.2 V. Meanwhile, the process conformed to the pseudo-first-order kinetic model with $R^2 \geq 0.95$, and the value of k increased with decreasing voltage. Noticeably, η (Table 1) showed a volcanic pattern with decreasing potential, with a maximum value of 26.9% at −1.2 V. The products were shown to be NH_4^+-dominated, and the selectivity was 86.8%, 90.5%, 85.4%, 91.2%, and 91.6 at −1.0, −1.1, −1.2, −1.3, and −1.4 V, respectively. As is well known, OVs can weaken N-O bonding, hindering the formation of byproducts [3]. Generally, the optimal applied potential of Co_3O_{4-x}/NF for NO_3RR was −1.2 V vs. Ag/AgCl.

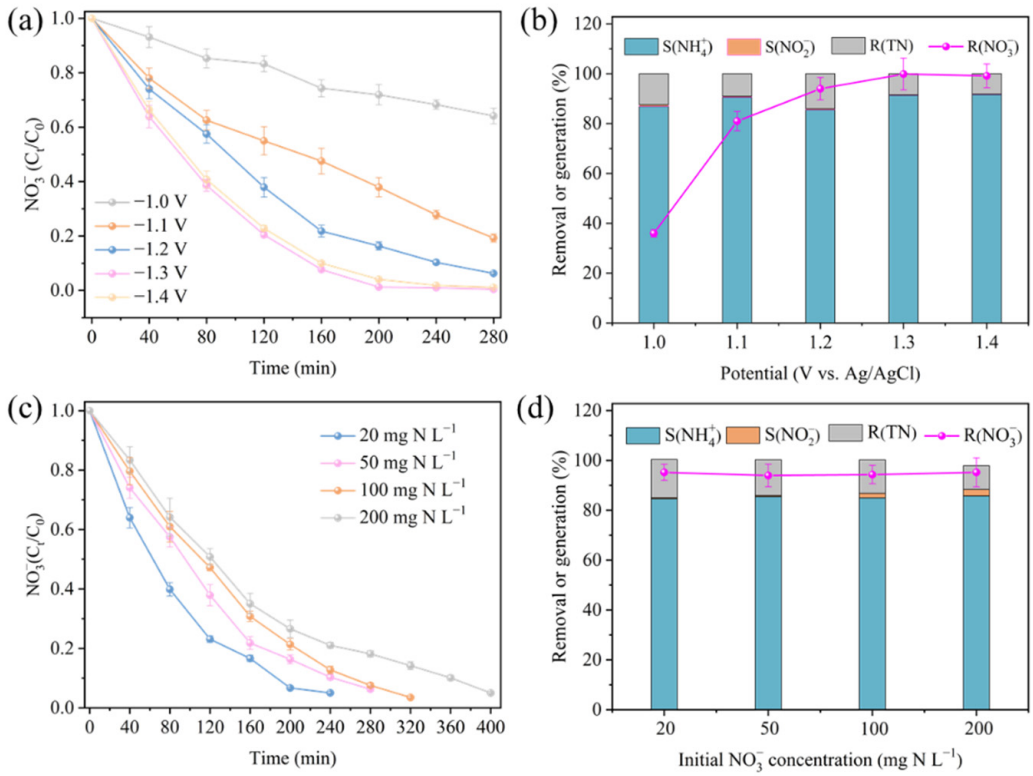

Figure 5. Effect of cathodic potential on NO_3^- reduction (**a**,**b**). Electrolysis conditions: Initial NO_3^- concentration = 50 mg N L^{-1}, Solution volume = 80 mL, pH = 7.0, Stirring rate = 600 rpm, Electrolysis time = 5 h; Effect of initial NO_3^- concentration on NO_3^- reduction (**c**) and removal or generation efficiency (**d**); Electrolysis conditions: Cathodic potential = −1.2 V (vs. Ag/AgCl), Solution volume = 80 mL, pH = 7.0, Stirring rate = 600 rpm, Electrolysis time = 5 h.

Table 1. Summary of electrochemical NO_3^- reduction with Co_3O_{4-x}/NF cathode.

	Cathodic Potential (V vs. Ag/AgCl) [a]					NO_3^- Concentration (mg N L^{-1}) [b]			
	−1.0	−1.1	−1.2	−1.3	−1.4	20 [c]	50	100 [d]	200 [e]
$R(NO_3^-)$	35.9	80.7	93.7	99.5	98.8	94.9	93.7	94.1	94.9
$S(NH_4^+)$	86.8	90.5	85.4	91.2	91.6	84.6	85.4	84.9	85.7
η [f]	11.5	24.6	26.9	24.5	22.8	12.3	26.9	36.5	45.9
k (min^{-1}) [g]	0.0016	0.0055	0.0102	0.0170	0.0210	0.0128	0.0102	0.0093	0.0069
R^2	0.98	0.97	0.99	0.98	0.95	0.98	0.99	0.98	0.97

[a] Initial NO_3^- concentration = 50 mg N L^{-1}, Initial pH = 7.0, Stirring rate = 600 rpm, Solution volume = 80 mL, Reaction time = 280 min; [b] Cathodic potential = −1.2 V (vs. Ag/AgCl), Initial pH = 7.0, Stirring rate = 600 rpm, Solution volume = 80 mL, Reaction time = 280 min; [c] Reaction time = 240 min; [d] Reaction time = 320 min; [e] Reaction time = 400 min; [f] η is the average current efficiency; [g] k is the pseudo-first-order kinetic rate constant.

Initial concentration is an important parameter for evaluating the application prospects of catalysts, and was accordingly investigated. Electrolysis reactions were performed under several initial NO_3^- concentration (20–200 mg N L^{-1}). Figure 5c shows that the NO_3^--N removal efficiency was 94.9%, 93.7%, 94.1%, and 94.9% for 20, 50, 100, and 200 mg N L^{-1}, respectively, at different reaction times, indicating that the Co_3O_{4-x}/NF electrode can be used for treating different NO_3^- concentrations in water. As mentioned in Table 1, η values increased with increasing NO_3^- concentrations; more specifically, the value of η was 12.3, 26.9, 36.5, and 45.9 at 20, 50, 100, and 200 mg N L^{-1}, which is due to the weakened competition in HER at relatively high nitrate concentrations [13]. NH_4^+ selectivity was consistently maintained ~85% at different NO_3^- concentrations, indicating that the Co_3O_{4-x}/NF electrode has outstanding potential for ammonia production via NO_3RR. Notably, as shown in Table 2, the Co_3O_{4-x}/NF electrocatalyst showed competitive NO_3^--N conversion and high NH_4^+ selectivity. The conversion of nitrate is a key aspect of wastewater treatment, with a high conversion rate indicating more effective purification. In our study, the Co_3O_{4-x}/NF electrode consistently achieved an NO_3^--N conversion rate over 93.7% across a range of nitrate concentrations, demonstrating its great potential for practical applications. The selectivity of NH_4^+-N is an important factor for the resourceful disposal of NO_3^- wastewater, as higher values indicate greater potential for useful applications. Our study found that the Co_3O_{4-x}/NF electrode consistently maintained an NH_4^+-N selectivity of approximately 85% across various nitrate concentrations, which exceeds the values reported in many previous studies [38–40]. To sum up, our study highlights the substantial practical application value of Co_3O_{4-x}/NF electrodes in the management of NO_3^--containing wastewater. Their consistently high NO_3^--N conversion rates and superior NH_4^+-N selectivity make them a promising candidate for resourceful disposal of these types of effluents.

Table 2. Comparison of NO_3RR performance between Co_3O_{4-x}/NF and reported catalysts.

Catalyst	NO_3^-—N Concentration (ppm)	NO_3^-—N Conversion (%)	NH_4^+—N Selectivity (%)	Ref.
Co_3O_{4-x}/NF	20	94.9	84.6	This work
	50	93.7	85.4	
	100	94.1	84.9	
	200	94.9	85.7	
Cu MNC-7	100	94.9	81.8	[38]
TiO_{2-x}/Ti foil	50	95.2	87.1	[3]
Fe_2O_3 NRs/CC	1400	<1	75.2	[26]
Co_3O_4@NiO	200	46	62.3	[39]
Fe SAC	7000	~7	69	[40]

3.4. Proposed Reaction Mechanism

To gain insights into the selective synthesis of NH_3 over Co_3O_{4-x}/NF, we conducted an XPS analysis to investigate the valence change of Co. In fact, the electrocatalytic activity

of cobalt oxide is closely related to its electronic states [30], and oxygen defect engineering as an effective mean for regulating the electronic state of materials has been generally confirmed by previous studies [31]. As shown in Figure 4, the introduction of OVs can significantly enhance both NH_3 production performance as well as the kinetics of the electrochemical reduction of NO_3^-. In addition, it is notable that the XPS results clearly show the Co^{2+}/Co^{3+} ratio increasing from 0.78 to 1.04 after the introduction of OVs. Therefore, it is reasonable to speculate that Co^{2+} plays a crucial role in NO_3^- reduction and NH_4^+ production. As shown in Figure 6a,b, the ratio of Co^{2+}/Co^{3+} in Co_3O_{4-x}/NF decreased to 0.85 after electrocatalytic reduction. Such changes not only indicate that the electrocatalytic reduction of NO_3^- is mediated by the Co^{2+}/Co^{3+} cycle, they show that Co^{2+} acts as the active site for transferring electrons to NO_3^- toward ammonia production. As a result, the OVs can regulate the conversion of Co^{3+} to Co^{2+}, which improves the poor conductivity of Co_3O_4 and provides more active sites, thereby enhancing the catalytic performance of the electrocatalytic reduction of NO_3^- into NH_3.

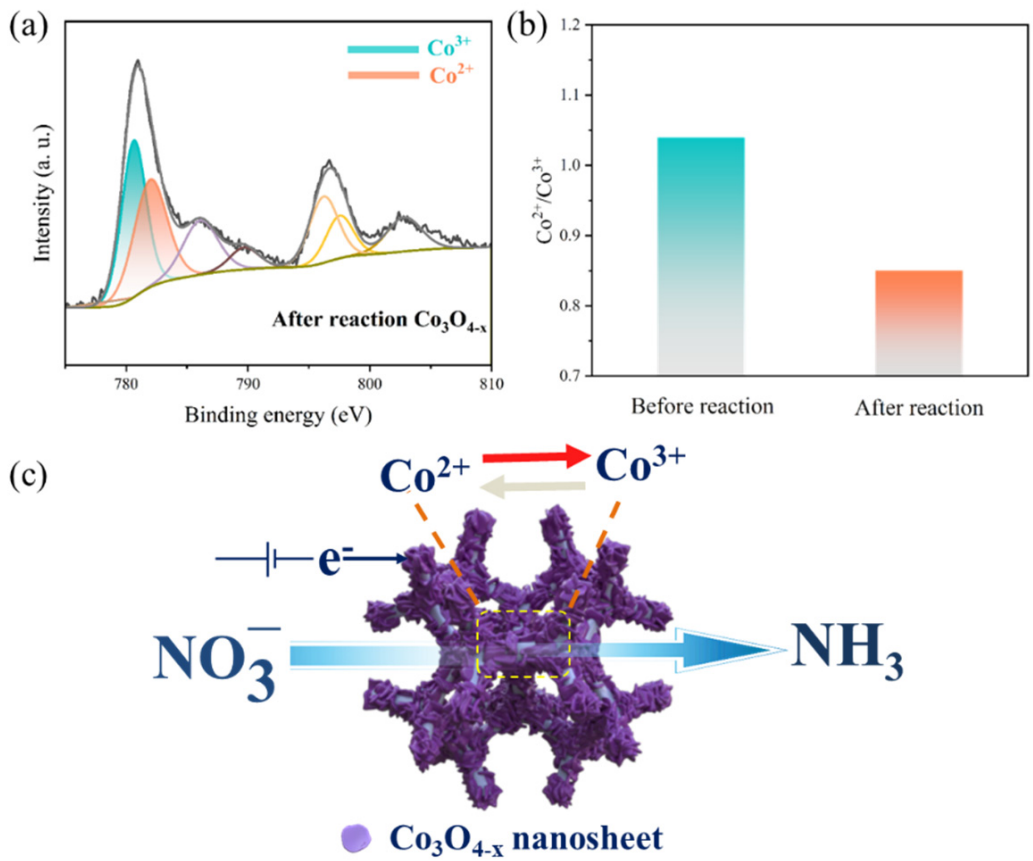

Figure 6. XPS spectra of Co 2p after the reaction (**a**), the Co^{2+}/Co^{3+} ratio before and after the reaction (**b**), and schematic diagram of the possible reaction mechanism (**c**).

4. Conclusions

In summary, Co_3O_4 nanosheets with OVs supported on nickel foam were successfully synthesized and demonstrated to be an efficient catalyst for NH_3 synthesis from NO_3^- electroreduction. At −1.2 V, 93.7% nitrate removal and 85.4% NH_3 production selectivity were obtained vs. Ag/AgCl. Compared with Co_3O_4/NF, the EIS and C_{dl} results confirmed that the introduction of OVs enhanced the electron transfer capability and ECSA of the electrode. In addition, the presence of OVs influenced the Co^{2+}/Co^{3+} ratio due to the reduction of Co^{3+} into Co^{2+}. The Co^{2+}/Co^{3+} cycle was identified as a key mediator in the electrocatalytic reduction of NO_3^- for NH_3 production. These results can shed light on the importance of the Co^{2+}/Co^{3+} ratio in the electrocatalytic synthesis of ammonia, and highlight the potential of oxygen-defective catalysts for developing more efficient and sus-

tainable electrocatalytic processes. The findings of our study suggest that electrochemical denitrification may hold promise for ammonia production; however, further research is necessary in order to maximize the utilization of NH_4^+ and enable its in situ recovery.

Supplementary Materials: The following supporting information can be downloaded at: https://www.mdpi.com/article/10.3390/met13040799/s1, Figure S1: CV curves of NF (a) and Co_3O_4/NF (b) in the range of −0.06~0.06 V vs. Ag/AgCl; Figure S2: The pseudo-first-order kinetic analyses.

Author Contributions: X.W.: Investigation, Formal analysis, Writing—original draft, Writing—review and editing; Z.L. (Zhigong Liu), T.G., J.T. and Z.L. (Zhizhuo Li): Writing—review and editing; Z.S., F.F. and C.Q.: Formal analysis; F.Y.: Formal analysis, Writing—original draft, Funding acquisition; C.T.: Formal analysis, Writing—original draft, Funding acquisition. All authors have read and agreed to the published version of the manuscript.

Funding: This research was financially supported by the Postdoctoral Innovation Talent Support Program of China Project (BX2021378), the China Postdoctoral Science Foundation (2021M703630), the Natural Science Foundation of Hunan Province (Nos. 2022JJ40622), and the Technology Innovation Guidance Project of Jiangxi Province, China (20212BDH81030).

Institutional Review Board Statement: Not applicable.

Informed Consent Statement: Not applicable.

Data Availability Statement: Not applicable.

Conflicts of Interest: The authors declare no conflict of interest.

References

1. Bhatnagar, A.; Sillanpää, M. A review of emerging adsorbents for nitrate removal from water. *Chem. Eng. J.* **2011**, *168*, 493–504. [CrossRef]
2. Duca, M.; Koper, M.T.M. Powering denitrification: The perspectives of electrocatalytic nitrate reduction. *Energy Environ. Sci.* **2012**, *5*, 9726–9742. [CrossRef]
3. Jia, R.; Wang, Y.; Wang, C.; Ling, Y.; Yu, Y.; Zhang, B. Boosting Selective Nitrate Electroreduction to Ammonium by Constructing Oxygen Vacancies in TiO_2. *ACS Catal.* **2020**, *10*, 3533–3540. [CrossRef]
4. Gao, J.; Jiang, B.; Ni, C.; Qi, Y.; Zhang, Y.; Oturan, N.; Oturan, M.A. Non-precious Co_3O_4-TiO_2/Ti cathode based electrocatalytic nitrate reduction: Preparation, performance and mechanism. *Appl. Catal. B Environ.* **2019**, *254*, 391–402. [CrossRef]
5. Zhang, S.; Li, M.; Li, J.; Song, Q.; Liu, X. High-ammonia selective metal–organic framework–derived Co-doped Fe/Fe_2O_3 catalysts for electrochemical nitrate reduction. *Proc. Natl. Acad. Sci. USA* **2022**, *119*, e2115504119. [CrossRef] [PubMed]
6. Min, X.; Wu, X.; Shao, P.; Ren, Z.; Ding, L.; Luo, X. Ultra-high capacity of lanthanum-doped UiO-66 for phosphate capture: Unusual doping of lanthanum by the reduction of coordination number. *Chem. Eng. J.* **2019**, *358*, 321–330. [CrossRef]
7. Theerthagiri, J.; Park, J.; Das, H.T.; Rahamathulla, N.; Cardoso, E.S.F.; Murthy, A.P.; Maia, G.; Vo, D.N.; Choi, M.Y. Electrocatalytic conversion of nitrate waste into ammonia: A review. *Environ. Chem. Lett.* **2022**, *20*, 2929–2949. [CrossRef]
8. Li, J.; Zhan, G.; Yang, J.; Quan, F.; Mao, C.; Liu, Y.; Wang, B.; Lei, F.; Li, L.; Chan, A.W.M.; et al. Efficient Ammonia Electrosynthesis from Nitrate on Strained Ruthenium Nanoclusters. *J. Am. Chem. Soc.* **2020**, *142*, 7036–7046. [CrossRef]
9. Chen, G.-F.; Yuan, Y.; Jiang, H.; Ren, S.-Y.; Ding, L.-X.; Ma, L.; Wu, T.; Lu, J.; Wang, H. Electrochemical reduction of nitrate to ammonia via direct eight-electron transfer using a copper–molecular solid catalyst. *Nat. Energy* **2020**, *5*, 605–613. [CrossRef]
10. Wang, Y.; Zhou, W.; Jia, R.; Yu, Y.; Zhang, B. Unveiling the Activity Origin of a Copper-based Electrocatalyst for Selective Nitrate Reduction to Ammonia. *Angew. Chem. Int. Ed.* **2020**, *59*, 5350–5354. [CrossRef]
11. Lv, C.; Zhong, L.; Liu, H.; Fang, Z.; Yan, C.; Chen, M.; Kong, Y.; Lee, C.; Liu, D.; Li, S.; et al. Selective electrocatalytic synthesis of urea with nitrate and carbon dioxide. *Nat. Sustain.* **2021**, *4*, 868–876. [CrossRef]
12. Daiyan, R.; Tran-Phu, T.; Kumar, P.; Iputera, K.; Tong, Z.; Leverett, J.; Khan, M.H.A.; Esmailpour, A.A.; Jalili, A.; Lim, M.; et al. Nitrate reduction to ammonium: From CuO defect engineering to waste NO_x-to-NH_3economic feasibility. *Energy Environ. Sci.* **2021**, *14*, 3588–3598. [CrossRef]
13. Chen, F.-Y.; Wu, Z.-Y.; Gupta, S.; Rivera, D.J.; Lambeets, S.V.; Pecaut, S.; Kim, J.Y.T.; Zhu, P.; Finfrock, Y.Z.; Meira, D.M.; et al. Efficient conversion of low-concentration nitrate sources into ammonia on a Ru-dispersed Cu nanowire electrocatalyst. *Nat. Nanotechnol.* **2022**, *17*, 759–767. [CrossRef]
14. Gao, J.; Shi, N.; Li, Y.; Jiang, B.; Marhaba, T.; Zhang, W. Electrocatalytic Upcycling of Nitrate Wastewater into an Ammonia Fertilizer via an Electrified Membrane. *Environ. Sci. Technol.* **2022**, *56*, 11602–11613. [CrossRef]
15. Chaplin, B.P.; Reinhard, M.; Schneider, W.F.; Schüth, C.; Shapley, J.R.; Strathmann, T.J.; Werth, C.J. Critical Review of Pd-Based Catalytic Treatment of Priority Contaminants in Water. *Environ. Sci. Technol.* **2012**, *46*, 3655–3670. [CrossRef]

16. Zhao, H.-P.; Ontiveros-Valencia, A.; Tang, Y.; Kim, B.-O.; VanGinkel, S.; Friese, D.; Overstreet, R.; Smith, J.; Evans, P.; Krajmalnik-Brown, R.; et al. Removal of multiple electron acceptors by pilot-scale, two-stage membrane biofilm reactors. *Water Res.* **2014**, *54*, 115–122. [CrossRef] [PubMed]
17. Gruber, N.; Galloway, J.N. An Earth-system perspective of the global nitrogen cycle. *Nature* **2008**, *451*, 293–296. [CrossRef] [PubMed]
18. Chauhan, R.; Srivastava, V.C. Electrochemical denitrification of highly contaminated actual nitrate wastewater by Ti/RuO_2 anode and iron cathode. *Chem. Eng. J.* **2020**, *386*, 122065. [CrossRef]
19. Canfield, D.E.; Glazer, A.N.; Falkowski, P.G. The Evolution and Future of Earth's Nitrogen Cycle. *Science* **2010**, *330*, 192–196. [CrossRef]
20. Li, P.; Jin, Z.; Fang, Z.; Yu, G. A single-site iron catalyst with preoccupied active centers that achieves selective ammonia electrosynthesis from nitrate. *Energy Environ. Sci.* **2021**, *14*, 3522–3531. [CrossRef]
21. Zeng, Y.; Priest, C.; Wang, G.; Wu, G. Restoring the Nitrogen Cycle by Electrochemical Reduction of Nitrate: Progress and Prospects. *Small Methods* **2020**, *4*, 12. [CrossRef]
22. Wang, L.; Xia, M.; Wang, H.; Huang, K.; Qian, C.; Maravelias, C.T.; Ozin, G.A. Greening Ammonia toward the Solar Ammonia Refinery. *Joule* **2018**, *2*, 1055–1074. [CrossRef]
23. Soloveichik, G. Electrochemical synthesis of ammonia as a potential alternative to the Haber–Bosch process. *Nat. Catal.* **2019**, *2*, 377–380. [CrossRef]
24. Guo, S.; Heck, K.; Kasiraju, S.; Qian, H.; Zhao, Z.; Grabow, L.C.; Miller, J.T.; Wong, M.S. Insights into Nitrate Reduction over Indium-Decorated Palladium Nanoparticle Catalysts. *ACS Catal.* **2018**, *8*, 503–515. [CrossRef]
25. Radjenovic, J.; Sedlak, D.L. Challenges and Opportunities for Electrochemical Processes as Next-Generation Technologies for the Treatment of Contaminated Water. *Environ. Sci. Technol.* **2015**, *49*, 11292–11302. [CrossRef]
26. Li, T.; Tang, C.; Guo, H.; Wu, H.; Duan, C.; Wang, H.; Zhang, F.; Cao, Y.; Yang, G.; Zhou, Y. In Situ Growth of Fe_2O_3 Nanorod Arrays on Carbon Cloth with Rapid Charge Transfer for Efficient Nitrate Electroreduction to Ammonia. *ACS Appl. Mater. Interfaces* **2022**, *14*, 49765–49773. [CrossRef] [PubMed]
27. Ghalkhani, M.; Irannejad, N.; Sohouli, E.; Keçili, R.; Hussain, C.M. Environmental applications of nanographitic carbon nitride. In *Nanoremediation*; Elsevier: Amsterdam, The Netherlands, 2023; pp. 187–227. [CrossRef]
28. Farooq, N.; Luque, R.; Len, T.; Osman, S.M.; Qureshi, A.M.; Nazir, M.A.; Rehman, A.U. Design of $SrZr_{0.1}Mn_{0.4}Mo_{0.4}Y_{0.1}O_3$-δ heterostructured with ZnO as electrolyte material: Structural, optical and electrochemical behavior at low temperatures. *Ceram. Int.* **2023**, *49*, 2174–2182. [CrossRef]
29. Huang, L.; Zhang, H.; He, Z.; Chen, J.; Song, S. In situ formation of nitrogen-doped carbon-wrapped Co_3O_4 enabling highly efficient and stable catalytic reduction of *p*-nitrophenol. *Chem. Commun.* **2020**, *56*, 770–773. [CrossRef]
30. Xu, L.; Jiang, Q.; Xiao, Z.; Li, X.; Huo, J.; Wang, S.; Dai, L. Plasma-Engraved Co_3O_4 Nanosheets with Oxygen Vacancies and High Surface Area for the Oxygen Evolution Reaction. *Angew. Chem. Int. Ed.* **2016**, *55*, 5277–5281. [CrossRef]
31. Zhang, Y.; Huang, X.; Li, J.; Bai, J.; Zhou, C.; Li, L.; Wang, J.; Long, M.; Zhu, X.; Zhou, B. Rapid Conversion of Co^{2+} to Co^{3+} by Introducing Oxygen Vacancies in Co_3O_4 Nanowire Anodes for Nitrogen Removal with Highly Efficient H_2 Recovery in Urine Treatment. *Environ. Sci. Technol.* **2022**, *56*, 9693–9701. [CrossRef]
32. Wang, Y.; Zhou, T.; Jiang, K.; Da, P.; Peng, Z.; Tang, J.; Kong, B.; Cai, W.-B.; Yang, Z.; Zheng, G. Reduced Mesoporous Co_3O_4 Nanowires as Efficient Water Oxidation Electrocatalysts and Supercapacitor Electrodes. *Adv. Energy Mater.* **2014**, *4*, 16. [CrossRef]
33. McCrory, C.C.L.; Jung, S.; Ferrer, I.M.; Chatman, S.M.; Peters, J.C.; Jaramillo, T.F. Benchmarking Hydrogen Evolving Reaction and Oxygen Evolving Reaction Electrocatalysts for Solar Water Splitting Devices. *J. Am. Chem. Soc.* **2015**, *137*, 4347–4357. [CrossRef]
34. Wang, X.; Li, X.; Mu, J.; Fan, S.; Chen, X.; Wang, L.; Yin, Z.; Tade, M.; Liu, S. Oxygen Vacancy-rich Porous Co_3O_4 Nanosheets toward Boosted NO Reduction by CO and CO Oxidation: Insights into the Structure–Activity Relationship and Performance Enhancement Mechanism. *ACS Appl. Mater. Interfaces* **2019**, *11*, 41988–41999. [CrossRef] [PubMed]
35. Lin, K.-Y.A.; Chen, B.-C. Efficient elimination of caffeine from water using Oxone activated by a magnetic and recyclable cobalt/carbon nanocomposite derived from ZIF-67. *Dalton Trans.* **2016**, *45*, 3541–3551. [CrossRef] [PubMed]
36. Liu, H.; Han, J.-L.; Yuan, J.; Liu, C.; Wang, D.; Liu, T.; Liu, M.; Luo, J.; Wang, A.; Crittenden, J.C. Deep Dehalogenation of Florfenicol Using Crystalline CoP Nanosheet Arrays on a Ti Plate via Direct Cathodic Reduction and Atomic H. *Environ. Sci. Technol.* **2019**, *53*, 11932–11940. [CrossRef] [PubMed]
37. Mao, R.; Li, N.; Lan, H.; Zhao, X.; Liu, H.; Qu, J.; Sun, M. Dechlorination of Trichloroacetic Acid Using a Noble Metal-Free Graphene–Cu Foam Electrode via Direct Cathodic Reduction and Atomic H. *Environ. Sci. Technol.* **2016**, *50*, 3829–3837. [CrossRef]
38. Xue, Y.; Yu, Q.; Ma, Q.; Chen, Y.; Zhang, C.; Teng, W.; Fan, J.; Zhang, W.-X. Electrocatalytic Hydrogenation Boosts Reduction of Nitrate to Ammonia over Single-Atom Cu with Cu(I)-N_3C_1 Sites. *Environ. Sci. Technol.* **2022**, *56*, 14797–14807. [CrossRef]
39. Wang, Y.; Liu, C.; Zhang, B.; Yu, Y. Self-template synthesis of hierarchically structured Co_3O_4@NiO bifunctional electrodes for selective nitrate reduction and tetrahydroisoquinolines semi-dehydrogenation. *Sci. China Mater.* **2020**, *63*, 2530–2538. [CrossRef]
40. Wu, Z.-Y.; Karamad, M.; Yong, X.; Huang, Q.; Cullen, D.A.; Zhu, P.; Xia, C.; Xiao, Q.; Shakouri, M.; Chen, F.-Y.; et al. Electrochemical ammonia synthesis via nitrate reduction on Fe single atom catalyst. *Nat. Commun.* **2021**, *12*, 2870. [CrossRef]